

# A Consensus-Based Secondary Control Strategy for Hybrid ac/dc Microgrids with Experimental Validation

Enrique Espina, *Graduate Student Member, IEEE*, Roberto Cárdenas-Dobson, *Senior Member, IEEE*, John W. Simpson-Porco, *Member, IEEE*, Doris Sáez, *Senior Member, IEEE*, and Mehrdad Kazerani, *Senior Member, IEEE*

**Abstract**—Secondary control strategies in hybrid ac/dc-microgrids have been conventionally designed independently for each side of the microgrid, neglecting the interaction between the ac and dc sides due to the power transferred through the interlinking converter. This has a negative effect on the power-sharing and dynamic response of the system. In this paper, a novel distributed secondary control strategy for hybrid ac/dc-microgrids is presented which coordinates the control actions of the ac and dc sides. The proposed control scheme simultaneously regulates ac-voltage magnitude and frequency, as well as the dc-voltage magnitude, by including the interlinking converters in the control strategy via a distributed consensus approach. This improves the power-sharing accuracy and secondary control restoration of the variables in both ac and dc sides of the microgrid. Moreover, the proposed methodology avoids the circulating currents which are typically produced in systems with multiple interlinking converters. Several simulation and experimental tests, such as load impacts and plug-and-play capability, are presented to validate the performance of the proposed control strategy using a 24 kW hybrid ac/dc-microgrid laboratory prototype.

**Index Terms**—Microgrids, Hybrid ac/dc Microgrid, Secondary Control, Distributed Control, Interlinking Converter.

## I. INTRODUCTION

**I**N RECENT years, the increasing global concerns regarding energy sustainability and environmental protection have accelerated the development of more environmentally-friendly and more efficient technologies in the energy field. Among the most important of such technologies are renewable energy sources (RESs) integrated as distributed generators (DGs), as

This work was supported in part by CONICYT/FONDECYT 1170683, and in part by ISCI ANID PIA/BASAL AFB180003. The work of E. Espina was supported by CONICYTPCHA/Doctorado Nacional/2017-21171858. The support of the AC3E ANID-BASAL Project FB0008 is also kindly acknowledged. (Corresponding author: Roberto Cárdenas-Dobson)

E. Espina is with the Department of Electrical Engineering, University of Santiago of Chile, Av. Ecuador 3519, Santiago, 9170124, Chile (e-mail: enrique.espinag@usach.cl).

R. Cárdenas-Dobson and D. Sáez are with the Department of Electrical Engineering, University of Chile, Tupper 2007, Santiago, 8370451, Chile. D. Sáez is also with the Instituto Sistemas Complejos de Ingeniería (ISCI), República 695, Santiago, Chile (e-mail: jesus.cardenas@uchile.cl, dsaez@ing.uchile.cl).

J. W. Simpson-Porco is with the Department of Electrical and Computer Engineering, University of Toronto, 10 King's College Road, Toronto, ON, M5S 3G4, Canada (e-mail: jwsimpson@ece.utoronto.ca).

M. Kazerani is with the Department of Electrical and Computer Engineering, University of Waterloo, Waterloo, ON, N2L 3G1, Canada (e-mail: mkazerani@uwaterloo.ca).

well as those related to energy storage systems (ESSs). When multiple DGs and ESSs are connected to a common electrical system, the concept of microgrid (MG) is introduced [1]–[4]. Considering the advantages of MGs (see [3]–[5]), much research effort has been devoted in recent years to developing control strategies for both ac and dc-MGs.

For the most part, ac-MGs and dc-MGs have been studied separately [4]–[9]. Recently, the study of hybrid ac/dc-MGs has attracted attention, as hybrid MGs allow for simplified integration of both ac and dc generation and load, as well as energy storage elements into one electrical system [10]–[12]. In a hybrid ac/dc-MG, an ac-MG and a dc-MG are interconnected through *interlinking converters (ICs)*, as shown in Fig. 1. Most importantly, hybrid ac/dc-MGs allow for fewer ac/dc conversions [13], leading to a reduction of power losses and an improvement in power quality. As an example, the number of diode-rectifiers in dc-loads, such as laptops and led lighting, is reduced when such devices are directly connected to the dc-MG [14].

Our focus in this paper is on secondary control, which is the middle layer of the standard hierarchical control architecture for MGs [3], [15]. The goal of the secondary control system is typically to restore the frequency (in an ac-MG) and the average MG voltage (in an ac- or dc-MG) to their nominal values, while maintaining power-sharing between units. Both centralized and distributed secondary control methods have been extensively studied for ac and dc-MGs, respectively [16]–[19]. A centralized MG control strategy is susceptible to single-point failure, and becomes increasingly complex to implement as the number of *DGs* in the MG increases; distributed MG controls overcome these architectural problems. Issues such as communication delays and data losses, which arise in distributed MG control, have also been addressed [20], [21]. However, unified distributed controllers for *hybrid ac/dc-MGs* have not yet been proposed or studied in the literature.

In [22], the use of normalized droop curves on both sides of the *IC* is proposed to generate the active power reference for the *IC*, in order to accomplish active power-sharing on both sides of the MG. However, secondary control is not considered in this strategy. In [23], the authors propose a decentralized control scheme for reliable autonomous operation in a hybrid three-port ac/dc/ds (distributed storage) MG. In this case, a fully decentralized control methodology is considered, which is performed in three stages: a local power-

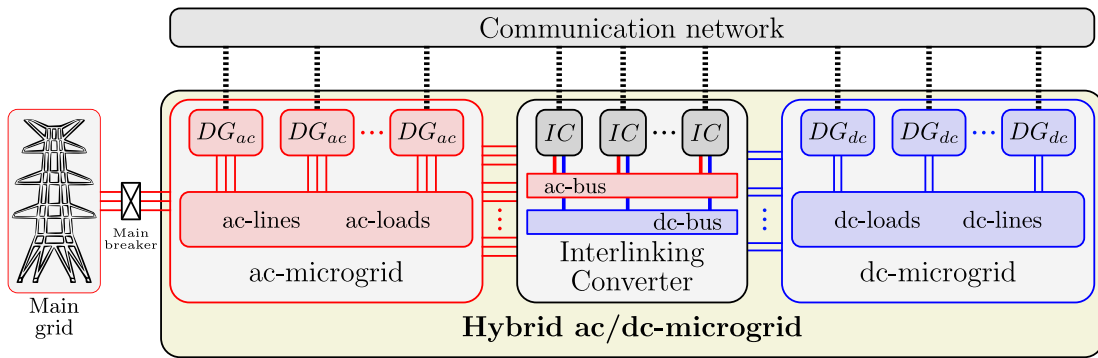


Fig. 1. General topology of a hybrid ac/dc-MG. If the main breaker is closed it is a ‘grid-tied’ MG, otherwise it is an ‘islanded’ MG.

sharing in each MG, a global power-sharing throughout MG, and power-sharing among ds systems. However, this strategy generates circulating currents among the  $ICs$ , which reduces the available current capability of the  $ICs$ .

Multiple  $ICs$  are considered in [24] based on the variable normalization discussed in [22]. To avoid circulating currents, the authors of [24] propose superimposing an ac component over the voltages on the dc-side of the  $ICs$ , to avoid circulating currents and achieve power-sharing between the  $ICs$ . This strategy however is complex to implement, and could require additional hardware, and secondary control systems are not discussed in [24].

In [25], the authors utilize the normalized droop curves discussed in [22], applying a secondary control system to restore the dc-voltage and frequency to the nominal values. Secondary control is implemented independently for each side, neglecting the coupling between the two sides of the hybrid MG caused by the power transferred through the  $IC$ . This has a negative impact on power-sharing on both sides, and on dynamic performance of the overall system. The time constants of the secondary controllers of the two sides have to be similar, as otherwise the power transferred through the  $IC$  may oscillate affecting the power-sharing.

In summary, there is relatively little literature on secondary control of hybrid ac-dc MGs, no comprehensive distributed control solutions are available, and no solutions are currently available which coordinate multiple  $ICs$  to prevent circulating currents. In this paper, a global Distributed Secondary Control (DSC) strategy, based on cooperative consensus (see [26]) for hybrid ac/dc-MGs is proposed. Power exchange between the ac and dc sides of the MG is realized by  $ICs$ , and is directly managed as part of our control strategy. To the best of the authors’ knowledge, the implementation of distributed secondary control strategies for hybrid ac/dc-MGs with multiple  $ICs$  has not been reported in the literature. Since we propose a *distributed control strategy*, a central controller is not required and the information is shared among neighbouring  $DGs$  only. Therefore, the communication layer is simplified (in comparison to a centralized communication network) and the plug-and-play capability of the hybrid MG is also improved.

The main contributions of the work presented in this paper can be summarized as follows:

- A coordinated DSC strategy for hybrid ac/dc-MGs is pro-

posed, which treats the hybrid MG as one electrical entity and not as three independent systems (i.e., ac, dc, and  $IC$ ).

- The proposed strategy achieves seamless restoration of the variables modified by the primary control at both sides of the hybrid MG. The dynamic coupling between the ac and dc sides due to the power transferred by the  $IC$  is not neglected, and the power-sharing capability of the  $DGs$  is not affected.
- The active powers transferred through the  $ICs$  are considered in the consensus functions and algorithms proposed in this work, which avoids circulating currents and achieves an accurate power-sharing between the  $ICs$ .
- The strategy achieves plug-and-play capability and robustness of the hybrid ac/dc-MG; power-sharing is achieved even if  $ICs$  (or  $DGs$ ) are connected or disconnected.
- The viability and effectiveness of the proposed control strategies have been validated using a 24kW hybrid ac/dc-MG prototype. A simulation study is also considered for including several scenarios which cannot be validated using the lab prototype, including scenarios with multiple  $ICs$ .
- An analytical model of the closed-loop system for the hybrid ac/dc-MG with the proposed consensus-based secondary control strategy is developed, which permits small-signal stability analysis and parameter tuning.

The rest of the paper is organized as follows. The distributed secondary control algorithms we propose for hybrid ac/dc-MGs are presented in Section II. The experimental results are given and extensively discussed in Section III. Simulation study and results are presented in Section IV. Finally, Section V provides some concluding comments.

## II. PROPOSED DISTRIBUTED SECONDARY CONTROL

A successful secondary control system should restore the secondary variables to their nominal values, and should improve (or, at least, not degrade) power-sharing between the  $DGs$ . In the DSC proposed in this paper, each  $DG$  will achieve *real power-sharing* with all other  $DGs$  of the hybrid MG, i.e., *ac-* and *dc-DGs*, and each *ac-DGs* will approximately achieve *reactive power-sharing* with all other *ac-DGs*.

We use the standard power-voltage ( $P/V$ ) droop controller [27] as the primary control system in the dc-MG, and the standard ( $P/f$ ) and ( $Q/V$ ) droop controllers [28] as the primary control systems in the ac-MG. As the frequency is a global variable in the ac-MG, accurate active power-sharing

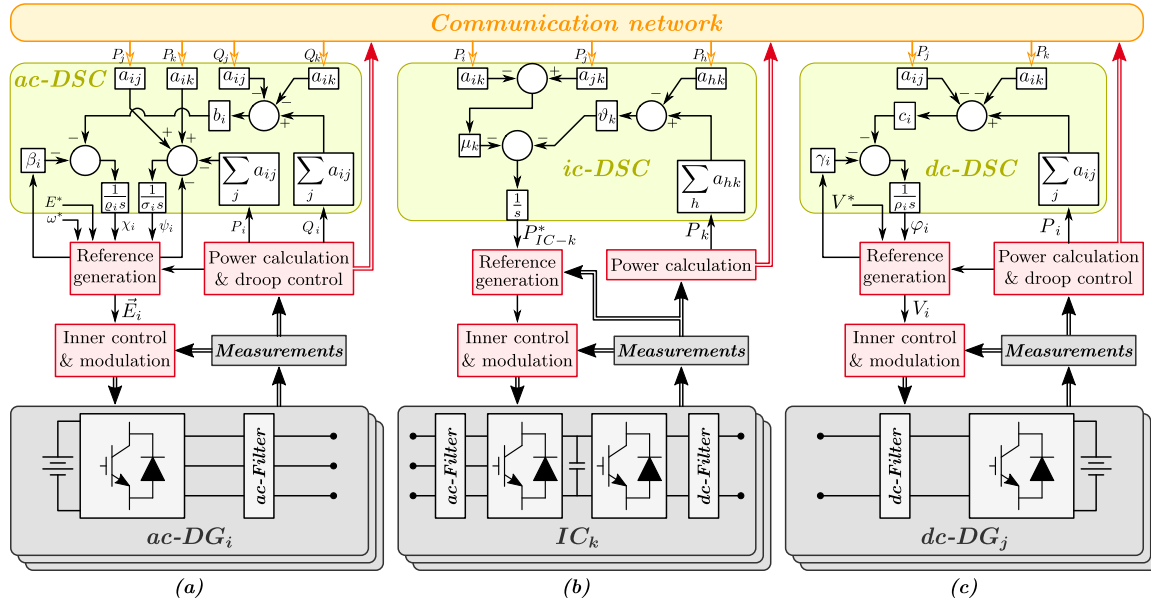


Fig. 2. Proposed distributed secondary control for: (a) ac-MG (ac-DSC), (b) IC (ic-DSC), (c) dc-MG (dc-DSC).

is achieved in the ac-MG. On the other hand, the amplitude of the voltages is a local variable. Thus, it is not possible to achieve both accurate power-sharing and voltage restoration simultaneously for each *DG* on either side of MG [16].

We consider a hybrid ac-dc MG consisting of *ac-DGs*, *dc-DGs*, and *ICs*, and we label the sets of these devices as  $\mathcal{N}_{ac} = \{1, \dots, n\}$ ,  $\mathcal{N}_{dc} = \{n + 1, \dots, n + m\}$ , and  $\mathcal{N}_{ic} = \{n + m + 1, \dots, n + m + g\}$ , respectively. A global secondary control strategy for hybrid ac/dc MGs should restore the secondary variables on both sides of the MG, and moreover, should ensure power-sharing between all *ac-DGs* and *dc-DGs*. To achieve the latter objective, the power flowing through the *IC* must be adjusted. We will introduce several distributed control mechanisms for achieving these goals. These control laws will use peer-to-peer communication between *dc-DGs*, *ac-DGs*, and *ICs*. To encode the communication topology, we let  $\mathbf{A}$  denote the *adjacency matrix* of a communication network between the *ac-DGs*, *dc-DGs*, and *ICs* (see, e.g., [16]). The elements of  $\mathbf{A}$  are 0 or 1, and  $a_{ij} = a_{ji} = 1$  means that units  $i$  and  $j$  can communicate with one another.

The time response of the proposed distributed secondary control strategy is strongly related to the density of matrix  $\mathbf{A}$ . Moreover, the time response is slow when  $\mathbf{A}$  is sparse, i.e., if most of the elements of  $\mathbf{A}$  are zero, while the time response is fast if the density of  $\mathbf{A}$  is high (most of the elements of  $\mathbf{A}$  are equal to 1). Therefore, unlike the case of centralized or decentralized secondary control strategies, in this case the time response also depends on the size and topology of the communication network.

In the following sections, we explain how DSC strategies are applied to *ac-DGs*, to *dc-DGs*, and to *ICs*.

#### A. DSC applied to the ac-MG (ac-DSC)

The secondary control loop for *ac-DGs* aims to restore the frequency  $\omega_i$  and the amplitude  $E_i$  of the ac-voltage to their

nominal values  $\omega^*$  and  $E^*$ , while maintaining satisfactory power-sharing. In our DSC, the communicated variables in the ac-MG are the active and reactive powers  $P_i$  and  $Q_i$  in p.u., which are given by

$$\begin{aligned} P_i &:= P_{ac-i}/S_{max-i}, & i \in \mathcal{N}_{ac}, \\ Q_i &:= Q_{ac-i}/S_{max-i}, & i \in \mathcal{N}_{ac}, \end{aligned} \quad (1)$$

where  $P_{ac-i}$  ( $Q_{ac-i}$ ) is the instantaneous real (reactive) power generated by the  $i$ th *ac-DG*, and  $S_{max-i}$  is the rated apparent power of the  $i$ th *ac-DG*. For the ac-MG, the secondary variables are the frequency ( $\omega_i$ ) and the amplitude ( $E_i$ ) of the voltages, while the consensus variables are the active power in p.u. ( $P_i$ ) and the reactive power in p.u. ( $Q_i$ ).

The ac-DSC for active power-sharing and frequency restoration is

$$\omega_i = \omega^* + M_{ac-i} P_{ac-i} + \psi_i \quad (2a)$$

$$\sigma_i \dot{\psi}_i = -(\omega_i - \omega^*) + \psi_{ac-i} + \psi_{dc-i} \quad (2b)$$

$$\psi_{ac-i} = -\sum_{j \in \mathcal{N}_{ac}} a_{ij} (P_{ac-i} - P_{ac-j}) \quad (2c)$$

$$\psi_{dc-i} = -\sum_{j \in \mathcal{N}_{dc}} a_{ij} (P_{ac-i} - P_{dc-j}) \quad (2d)$$

for  $i \in \mathcal{N}_{ac}$ , where  $P_{dc-j}$  is the instantaneous power generated by *dc-DG*  $j \in \mathcal{N}_{dc}$ .

The ac-DSC for reactive power-sharing and voltage restoration is

$$E_i = E^* + N_{ac-i} \cdot Q_{ac-i} + \chi_i \quad (3a)$$

$$\rho_i \dot{\chi}_i = -\beta_i (E_i - E^*) - b_i \sum_{j \in \mathcal{N}_{ac}} a_{ij} (Q_i - Q_j) \quad (3b)$$

for  $i \in \mathcal{N}_{ac}$ . The gains  $M_{ac-i}$ ,  $N_{ac-i} < 0$  are the primary droop gains, and  $\sigma_i, \rho_i > 0$  are time constants. The gains  $\beta_i, b_i > 0$  can be tuned to produce a compromise between voltage regulation accuracy and reactive power-sharing accuracy. A block diagram of the proposed distributed secondary control strategy for the *ac-DGs* is shown in Fig. 2(a). Although

relatively similar control strategies have been studied before (see [29]), the key difference is that we extend the active power consensus of *ac*-DGs to *dc*-DGs (and later, to ICs). This is reflected in the term  $\psi_{dc-i}$  [see (2d)], which illustrates the interaction between *ac*-DGs and *dc*-DGs, and in next sections.

### B. DSC applied to the *dc*-MG (*dc*-DSC)

The secondary control loop for *dc*-DGs aims to restore the dc voltages  $V_i$  to their nominal value  $V^*$  while maintaining satisfactory power-sharing. The variable shared by the *dc*-DGs is the power  $P_i$  in p.u. generated by the  $i$ th *dc*-DG, given by

$$P_i := P_{dc-i}/P_{max-i}, \quad i \in \mathcal{N}_{dc}, \quad (4)$$

for  $P_{dc-i}$  is the instantaneous power generated by the  $i$ th *dc*-DG and  $P_{max-i}$  is the rated power of the  $i$ th *dc*-DG. For the *dc*-MG, the secondary variable is the dc-voltage  $V_i$ , while the consensus variable is the p.u. power  $P_i$ . Our proposed *dc*-DSC for power-sharing and voltage restoration is

$$V_i = V^* + M_{dc-i} \cdot P_{dc-i} + \varphi_i \quad (5a)$$

$$\rho_i \dot{\varphi}_i = -\gamma_i (V_i - V^*) + \varphi_{dc-i} + \varphi_{ac-i} \quad (5b)$$

$$\varphi_{dc-i} = -c_i \sum_{j \in \mathcal{N}_{dc}} a_{ij} (P_{dc-i} - P_{dc-j}) \quad (5c)$$

$$\varphi_{ac-i} = -c_i \sum_{j \in \mathcal{N}_{ac}} a_{ij} (P_{dc-i} - P_{ac-j}) \quad (5d)$$

where  $i \in \mathcal{N}_{dc}$ ,  $M_{dc-i} < 0$  is the primary control gain, and  $\rho_i > 0$  is a time constant. The gains  $\gamma_i$  and  $c_i$  can be tuned to produce a trade-off between voltage regulation accuracy and power-sharing accuracy. A block diagram of the proposed *dc*-DSC is shown in Fig. 2(c).

### C. DSC for MGs with a single interlinking converter (*ic*-DSC)

The novel consensus-based DSC strategy for the ICs that we propose is slightly different than those used for *ac*-DGs and *dc*-DGs. The IC has to regulate the power transfer between the two sides of the MG. This has to be realized seamlessly, and without affecting the power-sharing among the DGs. To achieve this, the IC sends its own status (1: ON, 0: OFF) to the DGs in order to enable the power-consensus between the two sides of the MG, while the IC receives the power in p.u. being generated by the *ac*-DGs ( $P_{ac}$ ) and by the *dc*-DGs ( $P_{dc}$ ). The power reference  $P_{IC-k}^*$  for the single IC ( $k = n + m + 1$ ) is updated as<sup>1</sup>

$$\tau_k \dot{P}_{IC-k}^* = - \sum_{i \in \mathcal{N}_{ac}} \sum_{j \in \mathcal{N}_{dc}} a_{ik} a_{jk} (P_{ac-i} - P_{dc-j}) \quad (6)$$

where  $\tau_k > 0$  is a time constant. Note that the DGs communicating with the IC enter into the control law (6). A block diagram of the proposed *ic*-DSC is shown in Fig. 2(b).

From (6), note that the power reference for the IC will be adjusted to ensure power-sharing among DGs in both sides of the hybrid *ac/dc*-MG. Additionally, if the IC is out of service, it is possible to split the proposed control system into two

<sup>1</sup>The sign convention is that  $P_{IC-k}^* > 0$  if power flows from the *dc*-MG to the *ac*-MG.

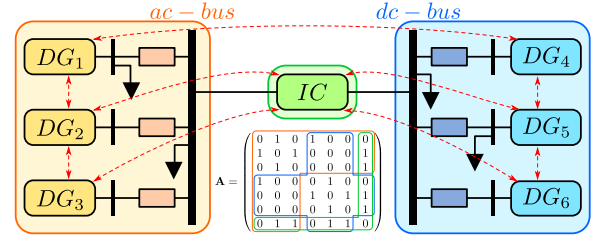


Fig. 3. Example topology of a hybrid *ac/dc*-MG with the adjacency matrix.

separate controllers (*ac*-DSC and *dc*-DSC), and change the global power-sharing to a sub-MG power-sharing. In this way, voltage/frequency regulation in each sub-MG can be achieved despite the temporary absence of the IC. Moreover, all the secondary control tasks are maintained within each MG, and the advantages of distributed controllers over the centralized ones are also maintained. However, if the lone IC in a hybrid *ac/dc*-MG fails, it will be impossible to transfer power from the *ac* side to *dc* side or vice-versa. Hence, the use of multiple ICs in hybrid *ac/dc*-MGs is highly recommended, as discussed in the next subsection.

Regarding the communication in (6), the proposed strategy works properly if at least one *ac*-DG and one *dc*-DG are communicating with the IC. This is illustrated using the hybrid MG topology shown in Fig. 3. Red dotted lines show the communication links between units. In this example, the hybrid *ac/dc*-MG is composed of 3 *ac*-DGs, 3 *dc*-DGs and 1 IC. The IC communicates with 2 DGs on each side of the MG. The adjacency matrix  $\mathbf{A}$  here models a connected bidirectional communication network.

### D. DSC for MGs with multiple interlinking converters

As mentioned before, by considering multiple ICs in the hybrid *ac/dc*-MG, it is possible to improve its reliability due to the existence of multiple paths for transferring power between sub-MGs. However, the existence of multiple ICs increases the complexity of the MG control and—depending on the control strategy utilized—can generate circulating currents among the ICs. These circulating currents must be eliminated to avoid overloading of converters or line congestion [24].

Thus, based on the single IC controller proposed in (6), an additional term to achieve a power consensus among multiple ICs is considered. The variable shared by the ICs is the power  $P_i$  in p.u. being transferred through the  $i$ th IC.

$$P_i := P_{IC-i}/P_{max-i}, \quad i \in \mathcal{N}_{ic}, \quad (7)$$

where  $P_{IC-i}$  is the instantaneous power through the  $i$ th IC and  $P_{max-i}$  is its rated power. The *ic*-DSC proposed in this work for the  $k$ th IC, considering  $g$  ICs in the MG, is given by

$$\begin{aligned} \dot{P}_{IC-k}^* = & -\mu_k \sum_{i \in \mathcal{N}_{ac}} \sum_{j \in \mathcal{N}_{dc}} a_{ik} a_{jk} (P_{ac-i} - P_{dc-j}) \\ & - \vartheta_k \sum_{h \in \mathcal{N}_{ic}} a_{hk} (P_k - P_h), \end{aligned} \quad (8)$$

where  $\mu_k$  and  $\vartheta_k$  are positive gains for adjusting the transient response and the accuracy of power-sharing. The proposed *ic*-DSC contributes to both power-sharing among DGs on the

two sides of the hybrid ac/dc-MG and power-sharing among *ICs*. Additionally, if any *IC* is out of service, the others can be used for transferring power between the two sub-MGs.

The ratio of power-sharing among *ICs* can also be controlled by adjusting the second term on the right side of (8). Nevertheless, to control this ratio, it is necessary to have a general knowledge of the hybrid ac/dc-MG and to perform additional studies (e.g., optimal power flow) which are typically utilized at the hierarchical tertiary control level. The tertiary control level is outside the scope of this paper.

### E. Closed-loop Model of Hybrid AC/DC Microgrid

An analytical model of the closed-loop system considering the proposed controllers is now developed for the purposes of small-signal stability analysis. The model for the experimental hybrid ac/dc-MG utilized in Section III, which is composed of  $\mathcal{N}_{ac}$  *ac-DGs*,  $\mathcal{N}_{dc}$  *dc-DGs* and 1 *IC*, is defined by the equations (2), (3), (5), (6), (9)-(12), and is illustrated in Fig. 4.

The power flows in the dc-MG are described by

$$p_{dc-ij}(V) = y_{ij}V_i(V_i - V_j) \quad (9a)$$

$$p_{dc-i}(V) = p_{dc-Di} + \sum_{j \in \mathcal{N}_{dc}} p_{dc-ij}(V) + s_i P_{IC} \quad (9b)$$

where  $p_{dc-ij}(V)$  is the power flow in the dc-line from bus  $i$  to bus  $j$ ,  $y_{ij}$  the line conductance, and  $V_i$  and  $V_j$  the dc-voltages at buses  $i$  and  $j$ , respectively. The active power supplied by the  $i$ th *dc-DG* ( $p_{dc-i}$ ) is given by (9b), where  $p_{dc-Di}$  corresponds to the power required by the load connected to bus  $i$ .

The active power flows in the ac-MG are characterized by

$$p_{ac-ij}(\theta, E) = \frac{R_{ij}E_i^2 - R_{ij}\Theta_{ij} + X_{ij}\Omega_{ij}}{R_{ij}^2 + X_{ij}^2} \quad (10a)$$

$$p_{ac-i} = p_{ac-Di} + \sum_{j \in \mathcal{N}_{ac}} p_{ac-ij}(\theta, E) - s_i P_{IC} \quad (10b)$$

$$\dot{\theta}_i = \omega_i \quad (10c)$$

$$\Theta_{ij} := E_i E_j \cos(\theta_i - \theta_j) \quad (10d)$$

$$\Omega_{ij} := E_i E_j \sin(\theta_i - \theta_j) \quad (10e)$$

where  $p_{ac-ij}(\theta, E)$  is the active power flow in the line from bus  $i$  to bus  $j$ ,  $R_{ij}$  and  $X_{ij}$  are the line parameters, and  $\Theta_{ij}$  and  $\Omega_{ij}$  are defined in (10d) and (10e), respectively. Finally,  $E_i$ ,  $\theta_i$  and  $\omega_i$  are the ac-voltage amplitude, angle and frequency at ac bus  $i$ . The active power supplied by the  $i$ th *ac-DG* ( $p_{ac-i}$ ) is given by (10b), where  $p_{ac-Di}$  corresponds to the active power required by the load connected to bus  $i$ , respectively. The active power contribution of the *IC* is reflected in (9b) and (10b) by the inclusion of the variable  $s_i$ , which is 1 if the *IC* is connected to bus  $i$  and 0 otherwise.

The reactive power flows in the ac-MG are as given by

$$q_{ij}(\theta, E) = \frac{X_{ij}E_i^2 - X_{ij}\Theta_{ij} - R_{ij}\Omega_{ij}}{R_{ij}^2 + X_{ij}^2} \quad (11a)$$

$$q_i = q_{Di} + \sum_{j \in \mathcal{N}_{ac}} q_{ij}(\theta, E) \quad (11b)$$

where  $q_{ij}(\theta, E)$  is the reactive power flow in the line from bus  $i$  to bus  $j$  and the remaining variables were previously explained. The reactive power supplied by the  $i$ th *ac-DG* ( $q_i$ )

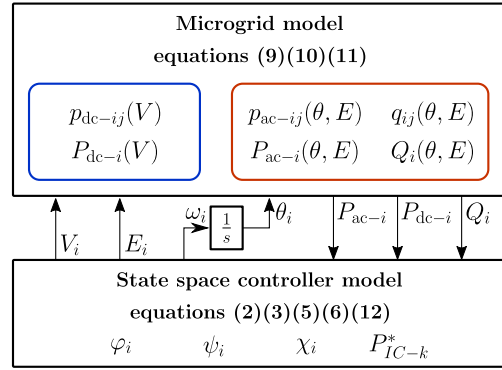


Fig. 4. Closed-loop system of the hybrid ac/dc-MG.

is given by (11b), where  $q_{Di}$  corresponds to the reactive power required by the load connected to bus  $i$ .

Finally, the low-pass-filters measurement typically utilized in primary (droop) control loop are considered, with a cut-off frequency of  $\omega_c$

$$\dot{P}_{dc-i} = -\omega_c(P_{dc-i} - p_{dc-i}) \quad (12a)$$

$$\dot{P}_{ac-i} = -\omega_c(P_{ac-i} - p_{ac-i}) \quad (12b)$$

$$\dot{Q}_i = -\omega_c(Q_i - q_i). \quad (12c)$$

The closed-loop model consists of the proposed distributed controllers (2), (3), (5), (6) and the microgrid model (9)-(12). Note that higher-bandwidth dynamics, such as inner current/voltage control loops, have been neglected in this model, as they are not relevant on the time-scale of secondary control. The obtained closed-loop model for the hybrid MG will be used for a small-signal stability analysis in Section III-C, to derive the stable limits for gains of proposed controllers and verify their tuning.

## III. EXPERIMENTAL RESULTS

### A. Experimental Setup

In order to experimentally validate the proposed control strategies, a 24kW hybrid ac/dc-MG laboratory prototype has been implemented in the MG lab at the University of Chile. The experimental rig is composed of five *Triphase*<sup>®</sup> power-electronic converters, which are utilized to emulate *DGs* in the ac-MG (*ac-DGs*) and in the dc-MG (*dc-DGs*), as well as the *IC*, and programmable ac-loads. The converters are communicating via optical fibre links and the control algorithms are implemented using control platforms based on Real-time Linux. The MG experimental setup is shown in Fig. 5. The topology utilized in this work is shown in Fig. 6 and its parameters are given in Table I and Table II, while the parameters of the controllers are given in Table III.

The inner (voltage and current) control loops implemented in each *DG* and *IC* were defined depending on the nature of the converter (ac or dc). Specifically, the inner and PR controllers suggested by *Triphase*<sup>®</sup> were tuned considering a bandwidth high enough to avoid coupling with the other control loops and to manage the transient changes in the frequency. However, since the main focus is the secondary control, the inner control level is considered out of the scope of this work.



Fig. 5. Experimental System based on five Triphase power converters with nominal powers between 5kW to 30kW (each one). They are configured to emulate the topology of Fig. 6.

TABLE I  
EXPERIMENTAL AC/DC-MG, GENERAL PARAMETERS.

Description	dc	ac	IC
# of DGs	6	3	1
Nominal Voltage (V)	150	110*	-
Frequency (Hz)	-	50	-
Nominal Power (kW/unit)	2.5	3.0	3.0
Switching frequency (kHz)	16		
Communication rate (Hz)	100		

\* Phase-to-neutral RMS voltage

TABLE II  
EXPERIMENTAL AC/DC-MG, PARAMETERS OF THE LINES.

Line	$\Omega$	Line	$\Omega$	Line	$\Omega$
$R_{12}$	0.67	$R_{34}$	0.50	$Z_{12}$	$0.10 + j0.79$
$R_{13}$	0.78	$R_{35}$	0.94	$Z_{13}$	$0.10 + j0.79$
$R_{24}$	0.50	$R_{46}$	0.47	$Z_{23}$	$0.10 + j0.79$

TABLE III  
PARAMETER OF THE CONTROLLERS.

Param.	dc-DGs	Param.	ac-DGs
$\gamma_i$	12.0 (1/s)	$1/\sigma_i$	50.0 (s)
$c_i$	50.0 (V/s)	$\beta_i$	12.0 (1/s)
$M_{dc-i}$	-3E-3 (V/W)	$b_i$	500.0 (V/s)
$\omega_c$	12.566 (rad/s)	$M_{ac-i}$	-2.1E-3 (rad/sW)
Param.	IC	$N_{ac-i}$	-1.8E-3 (V/VAr)
$1/\tau_i$	50.0 (1/W)	$\omega_c$	12.566 (rad/s)

The communication network of the hybrid ac/dc-MG is shown in Fig. 6. The white numbered circles (i.e., “bus dc- $j$ ” and “bus ac- $i$ ”) are showing the location where the DG loads are connected. The adjacency matrix ( $\mathbf{A}$ ) describing the communication network is given by (13a). In this matrix, element  $a_{ij} = 1$  if  $DG_i$  is communicating with  $DG_j$ ; otherwise,  $a_{ij} = 0$ . Rows (and columns) 1 to 6 show the communication links of the dc-MG, while rows (and columns) 7 to 9 show the communication links of the ac-MG. Communication links of the IC are shown in row (and column) 10. The matrix  $\mathbf{A}$  is composed of nine submatrices, as shown in (13b). For example; submatrix  $[\mathbf{dc}]_{6 \times 6}$  depicts the communication links within the dc-MG, while submatrices  $[\mathbf{dc-ac}]_{6 \times 3}$  and  $[\mathbf{dc-ic}]_{6 \times 1}$  represent the communication links between dc-MG and ac-MG, and between dc-MG and IC, respectively.

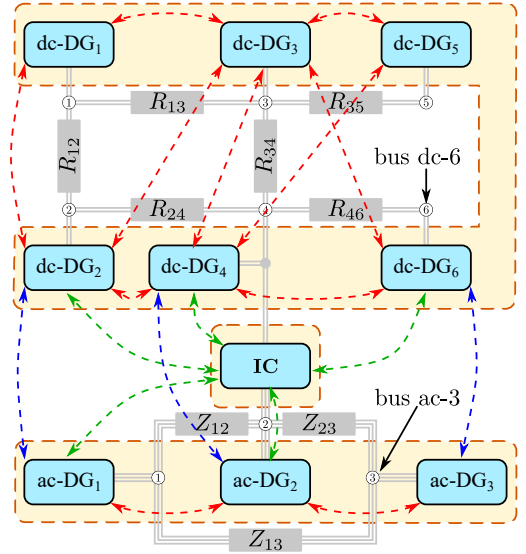


Fig. 6. Studied topology of the hybrid ac/dc-MG, including the communication channels between the DGs.

If all other controller parameters are equal (most importantly, the time constants), then more communication between DGs (i.e., a denser matrix  $\mathbf{A}$ ) leads to a faster response. In our tests, we assume the communication links available in the system are fixed, and the time responses of the secondary loops were adjusted to a common value of 2-3 seconds by tuning the gains  $\sigma_i$ ,  $\rho_i$  and  $\rho_i$ .

$$\mathbf{A} = \begin{pmatrix} 0 & 1 & 1 & 0 & 0 & 0 & 0 & 0 & 0 & 0 \\ 1 & 0 & 1 & 1 & 0 & 0 & 0 & 0 & 0 & 0 \\ 1 & 1 & 0 & 1 & 1 & 1 & 0 & 0 & 0 & 0 \\ 0 & 1 & 1 & 0 & 1 & 1 & 0 & 1 & 0 & 1 \\ 0 & 0 & 1 & 1 & 0 & 0 & 0 & 0 & 0 & 0 \\ 0 & 0 & 1 & 1 & 0 & 0 & 0 & 0 & 1 & 1 \\ 0 & 1 & 0 & 0 & 0 & 0 & 0 & 0 & 1 & 0 & 1 \\ 0 & 0 & 0 & 1 & 0 & 0 & 1 & 0 & 1 & 1 & 1 \\ 0 & 0 & 0 & 0 & 0 & 1 & 0 & 1 & 0 & 1 & 0 \\ 0 & 1 & 0 & 1 & 0 & 1 & 1 & 1 & 0 & 0 & 0 \end{pmatrix} \quad (13a)$$

$$= \begin{pmatrix} [\mathbf{dc}]_{6 \times 6} & [\mathbf{dc-ac}]_{6 \times 3} & [\mathbf{dc-ic}]_{6 \times 1} \\ [\mathbf{ac-dc}]_{3 \times 6} & [\mathbf{ac}]_{3 \times 3} & [\mathbf{ac-ic}]_{3 \times 1} \\ [\mathbf{ic-dc}]_{1 \times 6} & [\mathbf{ic-ac}]_{1 \times 3} & [\mathbf{ic}]_{1 \times 1} \end{pmatrix} \quad (13b)$$

The following approach was used for tuning the gains of the controllers. Firstly, all the controllers were considered active, and full-load conditions were assumed. Secondly, the root locus method using the closed-loop model derived in Section II-E was applied to the aforementioned operating condition. The following parameters were sequentially tuned: (i) the parameters related to the local voltages ( $\beta_i$ ,  $\gamma_i$ ) considering the other parameters are zero, (ii) the parameters associated with the active power consensus ( $\sigma_i$ ,  $c_i$ ,  $\tau_i$ ) considering ( $\beta_i$ ,  $\gamma_i$ ) as defined in (i), and (iii) the parameters corresponding to the reactive power consensus ( $b_i$ ) considering parameters obtained in (i) and (ii). Thirdly, several simulation scenarios were carried out to fine-tune the gains, changing the operating points to different loading conditions in order to analyze the bidirectionality of the power in the IC, and the results were satisfactory. If a more refined tuning of the controllers is required, meta-heuristic optimization techniques can be considered; however, this is out of the scope of this work.

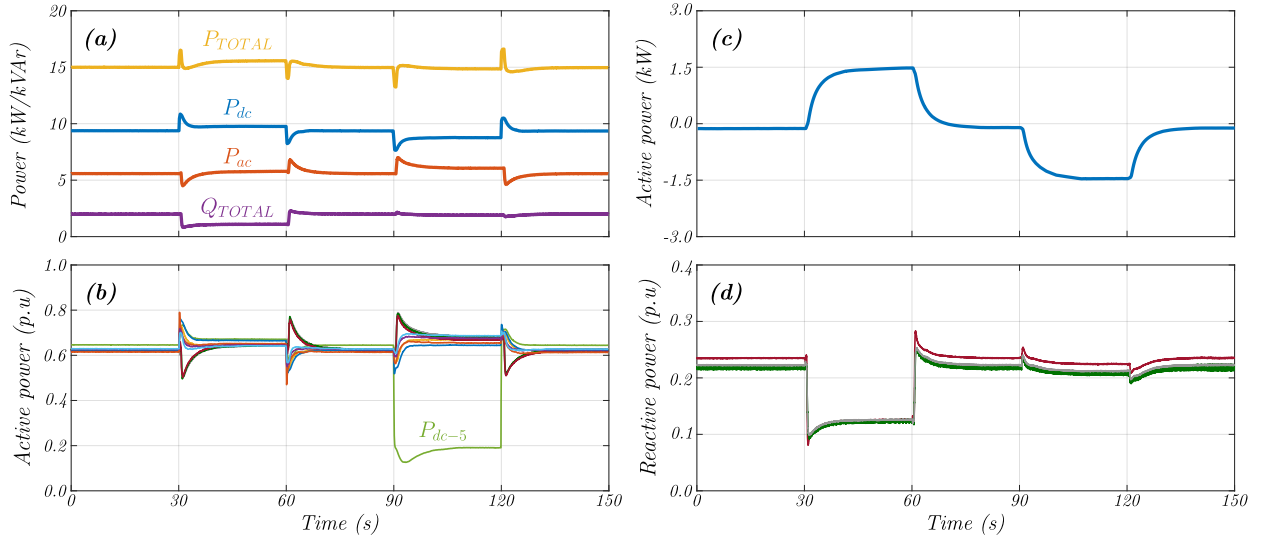


Fig. 7. Power in the hybrid ac/dc-MG for Test 1. (a) Total power (active and reactive). (b) Active power generated by  $ac$ -DGs ( $P_{ac-i}$ ,  $i = 1, 2, 3$ ) and  $dc$ -DGs ( $P_{dc-j}$ ,  $j = 1, \dots, 6$ ), in p.u. (c) Active power through the IC ( $P_{IC}$ ). (d) Reactive power generated by  $ac$ -DGs ( $Q_i$ ,  $i = 1, 2, 3$ ), in p.u.

## B. Experimental Tests

The experimental results obtained with the experimental rig described above are now presented. For all tests, all the control layers of the MG (i.e., inner, primary and secondary control loops) are active.

1) *Test 1 - Load Impact*: In this test, load changes are applied to both sides of the hybrid ac/dc-MG in order to validate (i) the proposed DSC, (ii) power-sharing among all DGs and (iii) bidirectional power flow through the IC. For this test, the initial load of the 9 DGs is summarized in Table IV. The total load of the hybrid ac/dc-MG is 15.3kW (9.6kW on dc-side and 5.7kW on ac-side) and 1.9kVAr, i.e., 63.75% of the nominal active power (24.0kW) and 21.1% of the nominal reactive power (9.0kVAr). The results are shown in Fig. 7(a).

TABLE IV  
EXPERIMENTAL AC/DC-MG, LOAD CONDITIONS OF TEST 1.

Load	kW	Load	kW	Load	kVA
$R_1$	2.05	$R_4$	2.05	$Z_1$	$0.0 + j0.8$
$R_2$	0.00	$R_5$	2.05	$Z_2$	$2.4 + j0.0$
$R_3$	1.37	$R_6$	2.05	$Z_3$	$3.3 + j1.1$

The power on the dc-side is 64.0% of the nominal power of this side (15.0kW); meanwhile, the active power on the ac-side corresponds to 63.3% of 9.0kW.

Because the secondary control loop is enabled, both  $ac$ -DGs and  $dc$ -DGs share almost perfectly the per unit (p.u.) power generated. The p.u. active powers of the nine DGs are shown in Fig. 7(b). As it is well known, the sharing of active power in the dc-side is compromised by the voltage regulation [see (5b)]. However, for  $t < 30s$ , the power-sharing of each  $dc$ -DG is still very good, with values between 0.646p.u. ( $dc$ -DG<sub>5</sub>) and 0.615p.u. ( $dc$ -DG<sub>2</sub>) and a total average (dc-side) of 0.628p.u. On the ac-side, the sharing of active power is almost perfect [see (2b)] with a value of about 0.624p.u. in each DG.

The power transferred through the IC is shown in Fig. 7(c). For  $t < 30$  the active power (in p.u.) on each side of the MG

is almost identical (64.0% dc and 63.3% ac). Therefore, the power transferred by the IC is negligible [see Fig. 7(c)]. The reactive power-sharing on the ac-side is shown in Fig. 7(d). In this case, there is a compromise between voltage regulation and reactive power-sharing [see (3b)]. The maximum reactive power corresponds to that of  $ac$ -DG<sub>1</sub> (for the whole test); meanwhile,  $ac$ -DG<sub>2</sub> and  $ac$ -DG<sub>3</sub> have almost equal values of normalized reactive power-sharing.

Secondary variables of the hybrid ac/dc-MG are shown in Fig. 8. It is concluded that the three secondary variables, i.e., the dc-voltage [see Fig. 8(a)], the ac-voltage [see Fig. 8(b)] and the frequency [see Fig. 8(c)] are maintained within the tolerance bands shown in black dashed line (allowable range for the voltages is  $V_{nom} \pm 5\%$  and for the frequency is  $f_{nom} \pm 2\%$ ). For  $t < 30s$  the lowest dc output voltage corresponds to  $dc$ -DG<sub>5</sub> and the highest corresponds to  $dc$ -DG<sub>2</sub> (no load is connected to the output of  $dc$ -DG<sub>2</sub>).

At  $t = 30s$  a load change is applied on both the ac-side and the dc-side. The load at node 2 on the dc-side is increased to 2.05kW, while the load at node 3 on the ac-side is decreased to  $1.8 + j0.0$ kVA. In this case, the p.u. load on the dc-side is higher than that on the ac-side. This is reflected in the power flow of the IC, as shown in Fig. 7(c). For  $30s < t < 60s$ , the active power transferred through the IC is  $P_{IC}^* = 1.5$ kW (the reactive power-sharing does not change). At  $t = 60s$ , the initial loading condition is resumed, i.e.,  $P_{IC}^* \approx 0$ kW.

At  $t = 90s$ , a new load change is applied on both ac and dc sides. The load at node 5 (dc-side) is step-decreased to 0.00kW, while the load at node 1 (ac-side) is step-increased to  $1.7 + j0.8$ kVA. Now, the percentage of ac-load is higher than that on the dc-side [see Fig. 7(c)]. Therefore, for  $90s < t < 120s$ ,  $P_{IC}^* = -1.5$ kW and the reactive power-sharing on the ac-side does not change [see Fig. 7(d)].

It is important to notice that, for  $90s < t < 120s$ , the  $dc$ -DG<sub>5</sub> [green line in Fig. 7(b)] is not participating in the power-sharing. In this time period, the load  $R_5$  is disconnected

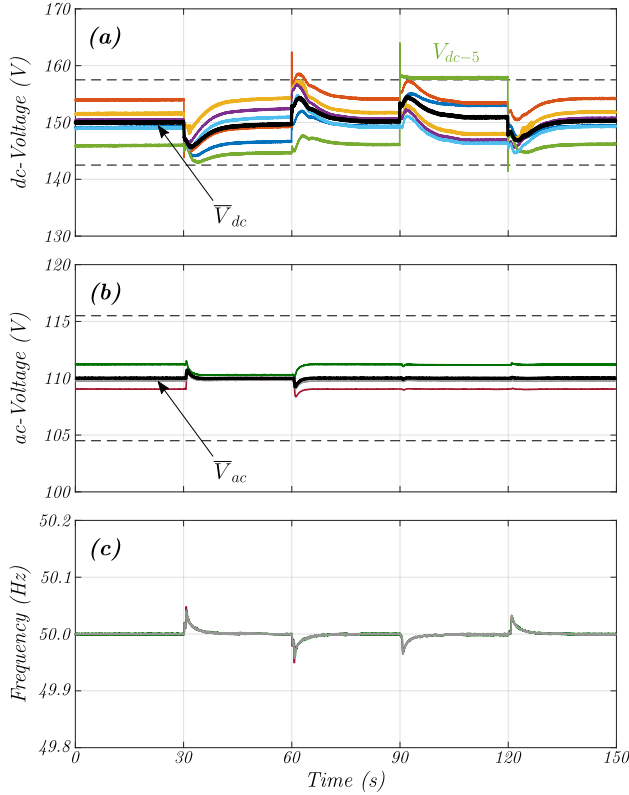


Fig. 8. Variables of the secondary control on the hybrid ac/dc-MG for Test 1. (a) Voltages on the  $dc$ -DGs ( $V_j, j = 1, \dots, 6$ ). (b) Phase-to-neutral RMS voltages on the  $ac$ -DGs ( $V_i, i = 1, 2, 3$ ). (c) Frequency of the voltages on the  $ac$ -DGs ( $f_i, i = 1, 2, 3$ ).

from node 5 on the dc-MG (see Fig. 6). Therefore, a high voltage is obtained at the  $dc$ -DG<sub>5</sub> output, when (5a)-(5b) are applied. Hence, it is not possible for this DG to participate in the power-sharing without surpassing the dc-voltage upper limit [see Fig. 8(a)]. This problem can be solved using the tertiary control system by, for instance, changing the value of  $V^*$  for all or some of the  $dc$ -DGs [see (5a)-(5b)]. However, tertiary control system is outside the scope of this work.

Finally, at  $t = 120s$  the loads are step-changed back to the initial condition until the end of the test ( $t = 150s$ ), i.e.,  $P_{IC}^* \approx 0kW$ , and all DGs participate in power-sharing.

2) *Test 2 - Loss of Unit:* In this test, the DGs on both sides of the hybrid MG and the IC are disconnected and then re-connected to test the plug-and-play capability of the proposed strategy. For this test, the load condition is summarized in Table V and it is not changed during the test. The total load of the hybrid ac/dc-MG is 16.5kW (9.6kW on dc-side and 6.9kW on ac-side) and 1.9kVAR, which represents 68.8% of the nominal active power (24.0kW) and 21.1% of the nominal reactive power (9.0kVAR), as shown in Fig. 9(a). The power on the dc-side corresponds to 64.0% of the nominal power of this side (15.0kW), while the active power on the ac-side is 76.7% of the nominal power of this side (9.0kW).

At  $t = 0s$ , both  $ac$ -DGs and  $dc$ -DGs are perfectly sharing the load power [see Fig. 9(b)]. Because the p.u. load on the ac-side is larger than that on the dc-side, the power flow in the IC is negative ( $P_{IC}^* \approx -0.8kW$ ), as shown in Fig. 9(c). The

TABLE V  
EXPERIMENTAL AC/DC-MG, LOAD CONDITIONS OF TEST 2.

Load	kW	Load	kW	Load	kVA
$R_1$	2.05	$R_4$	2.05	$Z_1$	$2.2 + j1.1$
$R_2$	0.00	$R_5$	2.05	$Z_2$	$2.4 + j0.0$
$R_3$	1.37	$R_6$	2.05	$Z_3$	$2.3 + j0.8$

reactive power-sharing on the ac-side is shown in Fig. 9(d). On the other hand, secondary variables of the hybrid ac/dc-MG are shown in Fig. 10. The three secondary variables, i.e., dc-voltage [Fig. 10(a)], ac-voltage [Fig. 10(b)] and frequency [Fig. 10(c)] are all maintained within the accepted limits.

At  $t = 20s$ ,  $dc$ -DG<sub>5</sub> fails and it is disconnected from both the MG and the communication network, and its power and voltage are reduced to zero (see green line in Fig. 9(b) and Fig. 10(a), respectively) and the other  $dc$ -DGs and  $ac$ -DGs maintain power-sharing and restoration of the secondary variables, as shown in Fig. 9(b), Fig. 9(d) and Fig. 10. Due to the absence of  $dc$ -DG<sub>5</sub>, the power transferred from the dc-side to the ac-side is reduced, as shown in Fig. 9(c).

At  $t = 40s$ ,  $ac$ -DG<sub>3</sub> fails and it is disconnected from both the MG and the communication network, and its power, voltage and frequency are all reduced to zero (see red line in Fig. 9(b) and yellow line in Fig. 10(b) and Fig. 10(c), respectively) and the remaining  $dc$ -DGs and  $ac$ -DGs maintain power-sharing and restoration of the secondary variables, as shown in Fig. 9(b), Fig. 9(d) and Fig. 10. Now, the absence of  $ac$ -DG<sub>3</sub> produces an increase in the power transferred from the dc-side to the ac-side, as shown in Fig. 9(c).

At  $t = 60s$ , the IC fails and it is disconnected from both the MG and the communication network, and its power is reduced to zero [see Fig. 9(c)]. This splits the hybrid MG into two independent systems; therefore, the power-sharing is now performed only among the units in the same sub-MG, as shown in Fig. 9(b). Because the p.u. load on the ac-side is higher than that on the dc-side, the p.u. powers generated by the  $ac$ -DGs are larger than those generated by the  $dc$ -DGs. On the other hand, the secondary variables are maintained within the operational limits all the time (see Fig. 10).

Finally, the failed units are reconnected to resume normal operation. The IC is reconnected at  $t = 80s$ , while  $dc$ -DG<sub>5</sub> is reconnected at  $t = 100s$  and  $ac$ -DG<sub>3</sub> at  $t = 120s$ . The MG continues operating as expected after each re-connection, maintaining both power-sharing and regulation of the secondary variables.

In summary, the experimental results demonstrate the advantages of the proposed method, which are:

- Active power consensus is achieved among the  $ac$ -DGs and  $dc$ -DGs when a load impact is applied on either side of the hybrid ac/dc-MG (see Fig. 7.b) and when a DG is connected/disconnected (see Fig. 9.b).
- The secondary control variables, i.e., average dc- and ac-voltages, and frequency, are restored to their nominal values in steady-state under all the analyzed cases (see Fig. 8 and Fig. 10).
- The IC participates actively in the proposed secondary control strategy, transferring power from the dc-side to

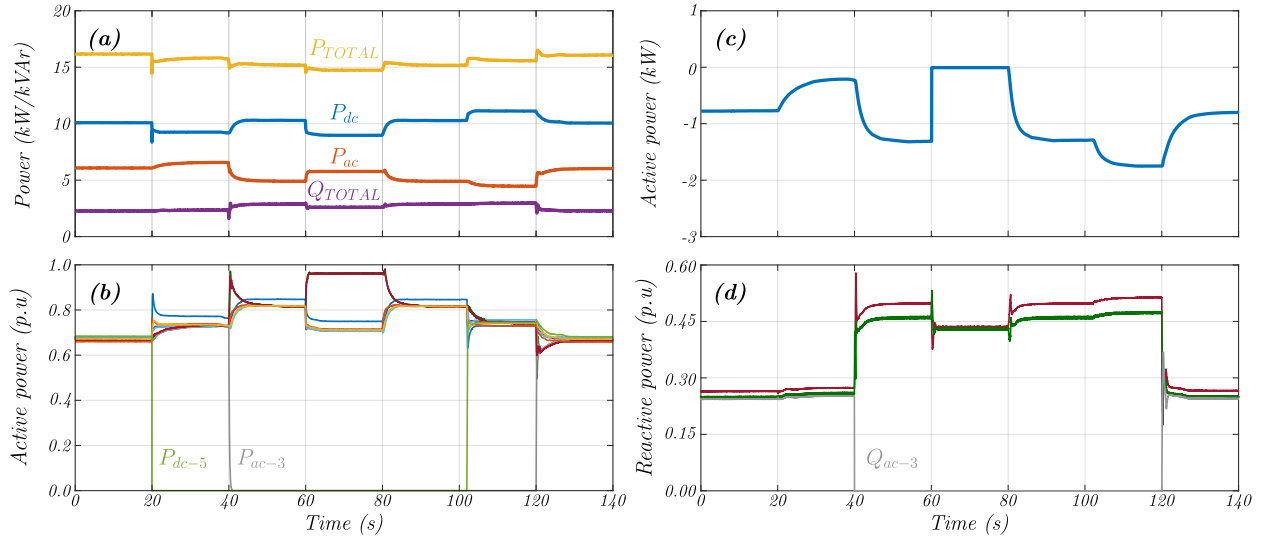


Fig. 9. Power on the hybrid ac/dc-MG for Test 2. (a) Total power (active and reactive). (b) Active power generated by *ac*-DGs ( $P_{ac-i}$ ,  $i = 1, 2, 3$ ) and *dc*-DGs ( $P_{dc-j}$ ,  $j = 1, \dots, 6$ ), in p.u. (c) Active power through the IC ( $P_{IC}$ ). (d) Reactive power generated by *ac*-DGs ( $Q_i$ ,  $i = 1, 2, 3$ ), in p.u.

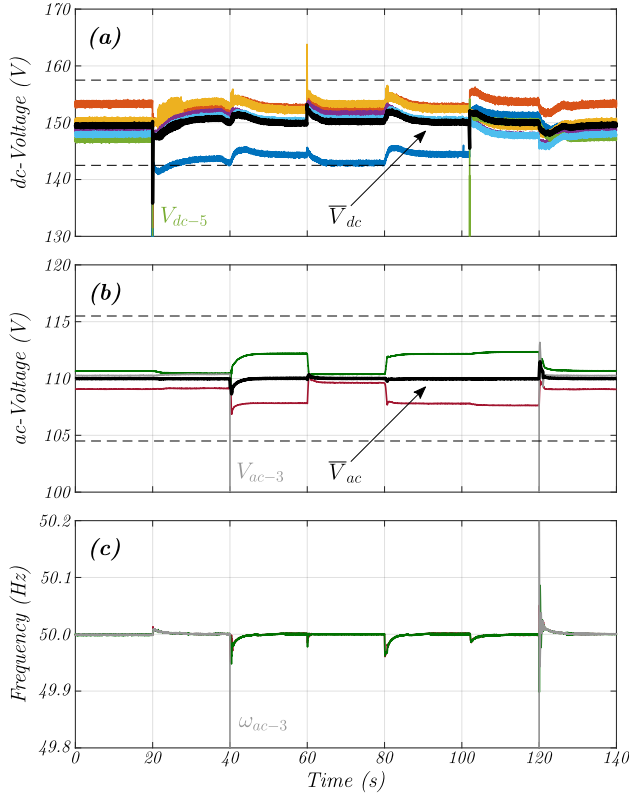


Fig. 10. Variables of the secondary control on the hybrid ac/dc-MG for Test 2. (a) Voltages on the *dc*-DGs ( $V_j$ ,  $j = 1, \dots, 6$ ). (b) Phase-to-neutral RMS voltages on the *ac*-DGs ( $V_i$ ,  $i = 1, 2, 3$ ). (c) Frequency of the voltages on the *ac*-DGs ( $f_i$ ,  $i = 1, 2, 3$ ).

the *ac*-side (or vice versa) according to the loading of the sub-MGs.

- The *DGs* can be easily connected to or disconnected from the MG as well as the distributed secondary control system, demonstrating the plug-and-play capability of the proposed strategy (see Test 2 results).

### C. Small-Signal Stability Analysis

To assess small-signal stability of the system under the proposed control strategy, eigenvalue analysis was performed on the closed-loop system model presented in Section II-E. Fig. 11 shows the eigenvalues obtained for the linearized closed-loop system at the operating point determined by the loading conditions in Table IV. The inset rectangle presents the zoom-in view of the slowest dominant eigenvalues. The arrows indicate the direction of movement of the eigenvalues as various controller gains are increased, as indicated in the legend. Note that, for reader's clarity, short trajectories are not shown since the effect of the parameters modified over the eigenvalue in that case is negligible. The control objectives analyzed are: (i) *ac*-voltage regulation [ $\beta_i$  in (3b)]; (ii) reactive power consensus [ $b_i$  in (3b)]; (iii) active power consensus [ $1/\sigma_i$  in (2b),  $c_i$  in (5b) and  $1/\tau_i$  in (6)]; and (iv) *dc*-voltage regulation [ $\gamma_i$  in (5b)].

From Fig. 11, it can be noted that the system is stable for the nominal values of the gains shown in Table III. On the other hand, the analysis of the eigenvalues trajectories permits to obtain critical values of the gains and state limits for the controller gains, in order to maintain the operation of the control system in the stable region. Moreover, by analyzing the participation factors [30], it is possible to conclude that the slowest eigenvalue  $\lambda = -0.168$  is strongly related to the state variable  $P_{IC}$ . The group of eigenvalues shown in the rectangle are mostly related to the variable  $\varphi_i$  [see (5b)]; thus the *dc*-voltages ( $V_{dc}$ ) present a slow dynamic in comparison to the secondary variables on the *ac*-MG ( $\omega$  and  $V_{ac}$ ). Further analysis can be realized by analyzing the participation factors.

A theoretical stability analysis is considered outside the scope of this work; nevertheless, the linearized system analysis performed in this section gives an adequate understanding of the hybrid ac/dc-MG's dynamic behaviour.

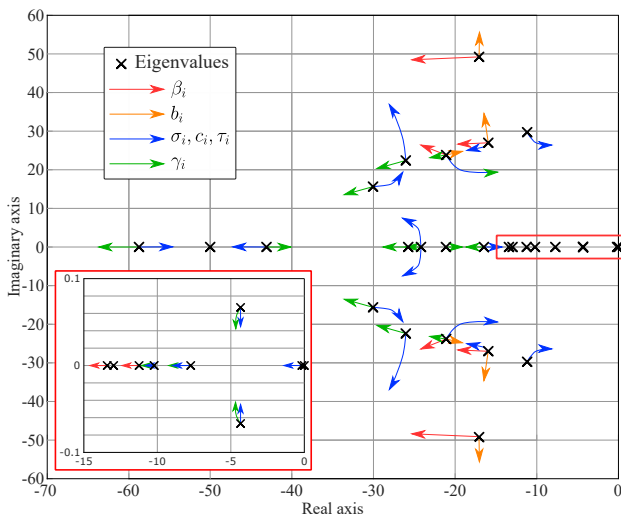


Fig. 11. Eigenvalues trajectory when increasing control system gains.

#### IV. SIMULATION RESULTS

In this Section, results of two simulation tests are presented. The first one (Section IV-A) compares the performance of the proposed strategy against those achieved by the control strategies presented in [22] and [25]. The second simulation test (Section IV-B) is utilized to analyze the performance of the proposed strategy considering a hybrid ac/dc-MG with multiple *ICs*. This could not be experimentally implemented in the lab, because a single *IC* was available in the *Triphase* MG.

##### A. Comparison test

As mentioned before, the performance of the proposed control strategy is compared to the performances obtained with strategies proposed in [22] and [25]. Load impacts and plug-and-play capabilities are studied using simulation work. For further details about the parameters and the topology of the simulated MG see Subsection III-A.

The results obtained using the control strategy presented in [22] are depicted in the left column of Fig. 12, while the results obtained with the strategy presented in [25] are shown in the central column of Fig. 12. The results obtained with the strategy proposed in this paper are illustrated in the right column of Fig. 12.

For simulation purposes, using strategies proposed in [22] and [25], each *ac*- and *dc*-*DG* is controlled using the strategies presented in Section II-A and Section II-B, respectively. However, for [22] secondary control is not applied. Additionally, for [22] and [25] the elements of the adjacency matrix given in (13a) are all zero since neither [22] nor [25] consider power consensus. On the other hand, the adjacency matrix used in the proposed strategy is shown in (13a).

To check the effects produced by the connection and disconnection of the *IC*, we disconnect it from the MG in two periods of time,  $35s < t < 75s$  and  $115s < t < 155s$ . Additionally, there are three load power scenarios in this test:

- $P_{dc} < P_{ac}$  :  $15s < t < 55s$
- $P_{dc} > P_{ac}$  :  $95s < t < 135s$
- $P_{dc} \approx P_{ac}$  : for the rest of the time

Firstly, when the *IC* is controlled using the strategy presented in [22], the power-sharing is not achieved between *DGs* located on different sides of the hybrid ac/dc-MG, even when the *IC* is connected [see Fig. 12(a)], and the secondary variables are not restored [see Fig. 12(c) and (14)]. Therefore, the power transferred through the *IC* [see Fig. 12(b)] is not utilized to achieve sharing of the per unit power on both sides.

Secondly, when the *IC* is controlled using the strategy proposed on [25], power-sharing is not achieved among *DGs* located on different sides of the hybrid ac/dc-MG [see Fig. 12(d)] although the secondary variables are restored to their nominal values [see Fig. 12(f)]. Furthermore, after the secondary variables are restored to their nominal values, the power transferred through the *IC* [see Fig. 12(e)] is negligible (the difference between the normalized values tends to be zero due to the secondary controllers).

Finally, if the *IC* is controlled using the strategy proposed in this work, it is capable of achieving good power-sharing among the *ac*- and *dc*-*DGs* [see Fig. 12(g)] while the *IC* is connected. If the *IC* is disconnected, the power-sharing is achieved within each sub-MG, dividing the controller into two independent sub-controllers. The *IC* and the proposed control system make it possible to achieve power-sharing between the *ac*-side and the *dc*-side, as shown in Fig. 12(h), while the secondary variables are well regulated [see Fig. 12(i)]. Although the normalized average voltage on the *dc*-side (see black dashed lines in the bottom row of Fig. 12) is not equal to the nominal value, the voltages are maintained within the operation limits due to the compromise between power consensus and voltage regulation.

The normalized frequencies ( $f_{pu}$ ) and voltages ( $V_{pu}$ ) shown in the bottom row of Fig. 12 are calculated using:

$$f_{pu} = \frac{f - \frac{1}{2}(f_{max} + f_{min})}{\frac{1}{2}(f_{max} - f_{min})}, \quad V_{pu} = \frac{V - \frac{1}{2}(V_{max} + V_{min})}{\frac{1}{2}(V_{max} - V_{min})}. \quad (14)$$

A summary of the comparison tests for strategies proposed in [22], [25] and the proposed strategy (P. S.) is shown in Table VI. By using [22], it is not possible to address the same control tasks that can be addressed by the proposed strategy. This is evident since [22] only equalizes the normalized dc-voltage and frequency at two ports of the *IC* without any secondary control strategy. Therefore, the *IC* only cares about its local variables and the power-sharing solely depends on the droop controls applied, which is a drawback when MGs have a large number of buses. By using [25], the secondary control is applied restoring the secondary variables. However, the power consensus between *ac*- and *dc*-*DGs* is not achieved since the *IC* only equalizes its local normalized variables. In contrast, the proposed strategy restores secondary variables while achieving power consensus between *ac*- and *dc*-*DGs*. This power consensus is reached as long the *IC* is working, i.e., as long as the path for transferring energy exists.

##### B. Operation with multiple *ICs*

In this subsection, the performance of the proposed control methodology is evaluated when three *ICs* and six *DGs*, on

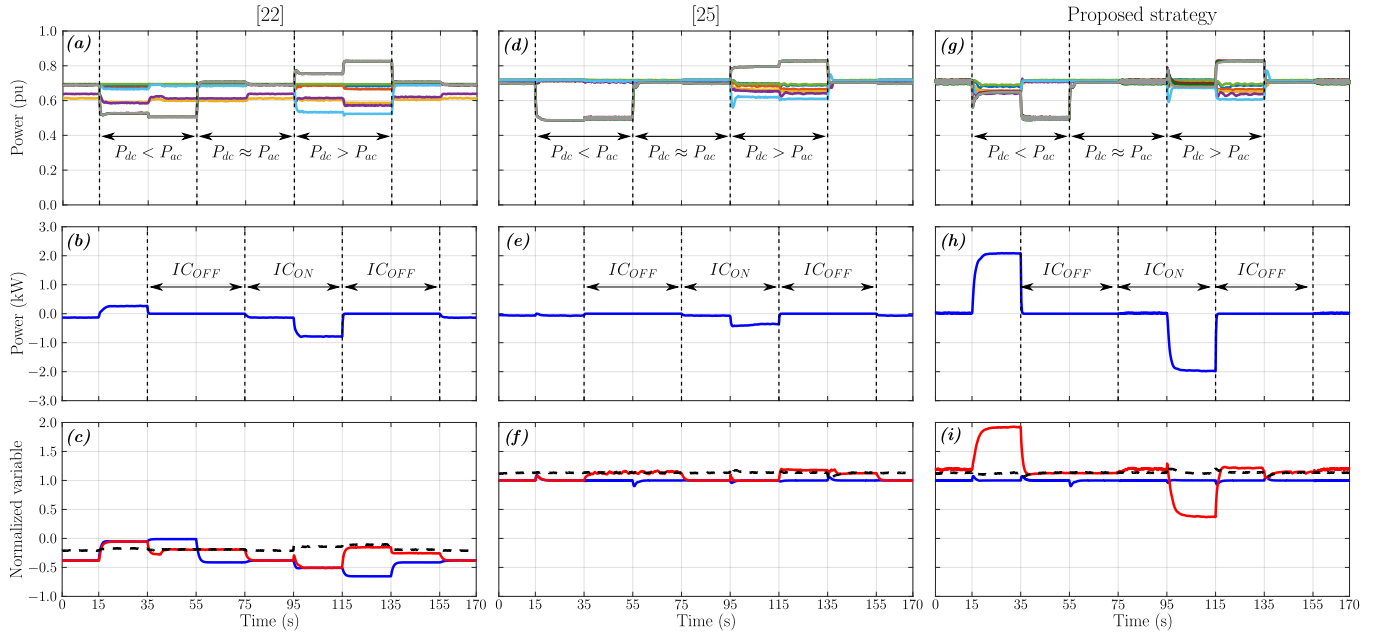


Fig. 12. Simulation test results for the comparison of the proposed strategy against the ones reported in [22] and [25]. *Top row*: Active power in p.u. generated by ac- and dc-DGs. *Middle row*: Active power transferred by the IC. *Bottom row*: Normalized dc-voltage (in red) and normalized frequency (in blue) on both sides of the IC, the black dashed lines show the *normalized average dc-voltage* in the dc-MG.

TABLE VI  
COMPARISON TEST SUMMARY.

	[22]	[25]	P. S.
Power-consensus, IC working	✗	✗	✓
Frequency restoration	✗	✓	✓
dc-voltage restoration	✗	✓	✓

each side of the hybrid ac/dc-MG, are considered. The studied topology is shown in Fig. 13(a).

Two scenarios are analyzed. Firstly, the operation of the proposed controller presented in Section II-C is evaluated (central column in Fig. 13), i.e., power-consensus among ICs is not considered in this test. Secondly, the proposed control methodology presented in Section II-D (including power-consensus among ICs), is simulated with the results being shown in the right column of Fig. 13.

For  $t < 10s$ , the ICs are not connected to the hybrid ac/dc-MG, i.e., the ac-side is not connected to the dc-side and the power-sharing among DGs on both sides of the MG is not active. Note that for  $t < 60s$ , the load power on the ac-side is higher than the load power on the dc-side [see Fig. 13(b)&(e)]. At  $t = 10s$ ,  $IC_1$  is connected and active power is transferred from the dc-side to ac-side initiating power-consensus between the ac- and dc-DGs. In this case, the control system performance is similar for both scenarios, considering that a single IC is connected.

At  $t = 20s$ ,  $IC_2$  is connected. The power-consensus among ac- and dc-DGs is maintained but the power-consensus between  $IC_1$  and  $IC_2$  is not achieved in the first scenario, but it is achieved in the second one (see Fig. 13(c)&(f)). At  $t = 30s$ ,  $IC_3$  is activated and the same results in terms of power-sharing among the ICs are obtained. The power-consensus among ICs in the first scenario is not achieved because, when the IC is

connected, the power-consensus among DGs on both sides has already been achieved. Therefore  $P_{1C}^*$  is not modified for  $IC_1$  (see (6)).

Then,  $IC_1$ ,  $IC_2$  and  $IC_3$  are disconnected at  $t = 40s$ ,  $t = 50s$  and  $t = 60s$ , respectively. In both scenarios the power-consensus among DGs is maintained and the power-sharing among ICs is also achieved. In the first scenario, the latter is achieved because the parameters of the controllers are the same for each IC; otherwise power-sharing among ICs is not ensured. Finally, at  $t = 70s$ , a load impact is applied and the load power on the dc-side is higher than the load power on the ac-side. At  $t = 80s$ , all the ICs are connected at the same time and both power-consensuses are achieved. Note that, in both scenarios, the secondary variables are correctly regulated, as shown in Fig. 13(d)&(g).

It is important to clarify that the proposed power consensus strategy for the ICs [see (8)] does not produce a circulating power between them. Therefore, it is not necessary to utilize auxiliary ac control signals as it is discussed in [24]. The methodology utilized to achieve power-consensus among the ICs eliminate any possible mismatch in the power flow transferred through the ICs.

## V. CONCLUSION

In this paper, a global distributed secondary control strategy for hybrid ac/dc-MGs has been proposed. This strategy considers the hybrid ac/dc-MG as a single entity, not three independent ones interacting with each other. The strategy is capable of restoring the variables modified by the primary control loop to their nominal values, while maintaining an accurate power-sharing among DGs on both sides of the microgrid. Additionally, when the hybrid ac/dc-MG has multiple ICs, accurate power-sharing among them is also ensured.

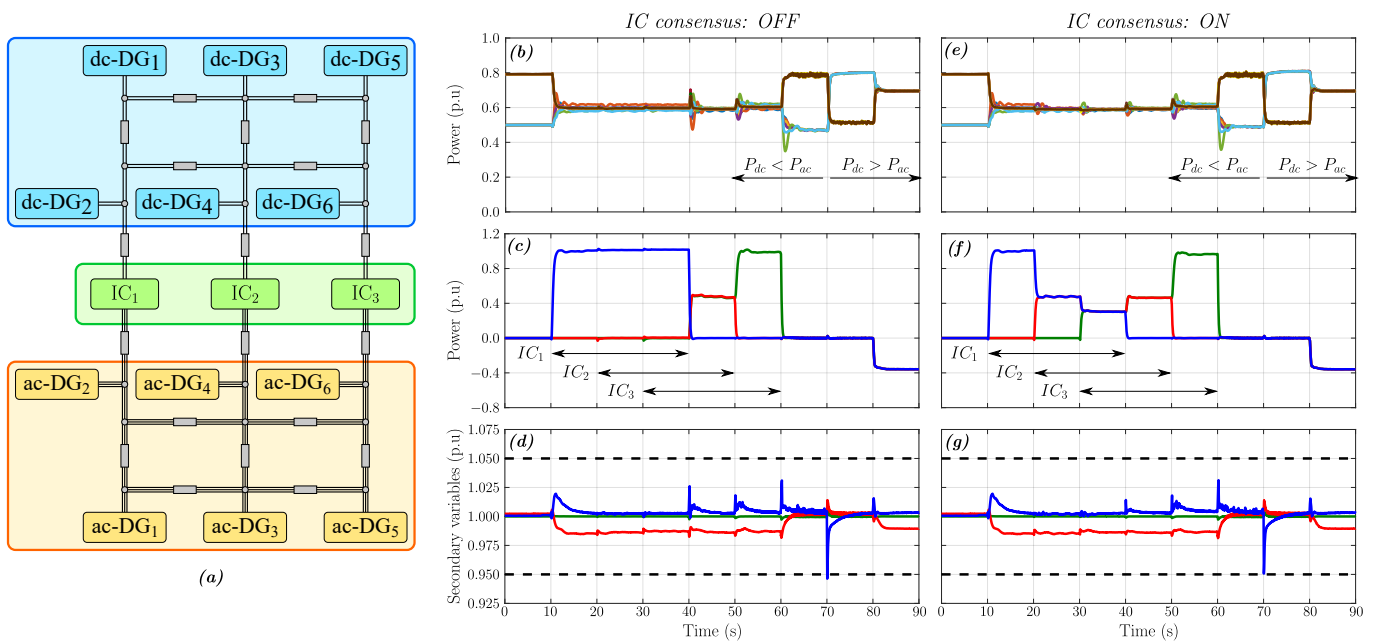


Fig. 13. Simulation test results considering multiple  $IC$ s in the hybrid ac/dc-MG. (a) Topology of the simulated MG. (b)&(e) Active power in p.u. generated by the ac- and dc-DGs. (c)&(f) Active power in p.u. transferred through the  $IC$ s. (d)&(g) Secondary variables in per unit, ac-side frequency (green), ac-voltage (red) and dc-voltage (blue).

The proposed strategy considers a reduced communication layer, as each  $DG$  is communicating only with its neighbouring  $DG$ s. Due to the fact that  $IC$ s also participate in the communication layer, the secondary control strategy can be adapted to each side separately in case the  $IC$ s are not available.

An analytical model of the closed-loop system of a hybrid ac/dc-microgrid with the proposed consensus-based secondary control strategy was derived for analyzing small-signal stability and tuning of the parameters of proposed controllers. The model was derived with the hybrid ac/dc-microgrid as a single entity, considering the interaction of the ac-DGs and dc-DGs via the power transfer through the  $IC$ .

Several experimental tests were realized using an experimental 24kW hybrid ac/dc-microgrid to demonstrate the effectiveness of the proposed control strategy in cases of load changes and connection/disconnection of  $DG$ s. Moreover, several simulation tests were realized to validate the application of the proposed controller when considering multiple  $IC$ s and to compare the behaviour of the proposed controller against those of the techniques reported in the literature. The performance of the controller in all the cases was excellent.

## REFERENCES

- [1] R. H. Lasseter, "MicroGrids," in *2002 IEEE Power Eng. Soc. Winter Meeting. Conf. Proc. (Cat. No.02CH37309)*, vol. 1, 2002, pp. 305–308 vol.1.
- [2] N. Hatzigiargyriou, H. Asano, R. Iravani, and C. Marnay, "Microgrids," *IEEE Power Energy Mag.*, vol. 5, no. 4, pp. 78–94, July 2007.
- [3] J. M. Guerrero, J. C. Vasquez, J. Matas, L. G. de Vicuna, and M. Castilla, "Hierarchical Control of Droop-Controlled AC and DC Microgrids—A General Approach Toward Standardization," *IEEE Trans. Ind. Electron.*, vol. 58, no. 1, pp. 158–172, Jan 2011.
- [4] D. E. Olivares, A. Mehrizi-Sani, A. H. Etemadi, C. A. Canizares, R. Iravani, M. Kazerani, A. H. Hajimiragha, O. Gomis-Bellmunt, M. Saeedifard, R. Palma-Behnke, G. A. Jiménez-Estévez, and N. D. Hatzigiargyriou, "Trends in Microgrid Control," *IEEE Trans. Smart Grid*, vol. 5, no. 4, pp. 1905–1919, July 2014.
- [5] T. Dragičević, X. Lu, J. C. Vasquez, and J. M. Guerrero, "DC Microgrids—Part I: A Review of Control Strategies and Stabilization Techniques," *IEEE Trans. Power Electron.*, vol. 31, no. 7, pp. 4876–4891, July 2016.
- [6] R. Majumder, B. Chaudhuri, A. Ghosh, R. Majumder, G. Ledwich, and F. Zare, "Improvement of Stability and Load Sharing in an Autonomous Microgrid Using Supplementary Droop Control Loop," *IEEE Trans. Power Syst.*, vol. 25, no. 2, pp. 796–808, May 2010.
- [7] J. M. Guerrero, M. Chandorkar, T. L. Lee, and P. C. Loh, "Advanced Control Architectures for Intelligent Microgrids—Part I: Decentralized and Hierarchical Control," *IEEE Trans. Ind. Electron.*, vol. 60, no. 4, pp. 1254–1262, April 2013.
- [8] T. Dragičević, J. M. Guerrero, J. C. Vasquez, and D. Škrlec, "Supervisory Control of an Adaptive-Droop Regulated DC Microgrid With Battery Management Capability," *IEEE Trans. Power Electron.*, vol. 29, no. 2, pp. 695–706, Feb 2014.
- [9] T. Dragičević, X. Lu, J. C. Vasquez, and J. M. Guerrero, "DC Microgrids—Part II: A Review of Power Architectures, Applications, and Standardization Issues," *IEEE Trans. Power Electron.*, vol. 31, no. 5, pp. 3528–3549, May 2016.
- [10] X. Liu, P. Wang, and P. C. Loh, "A Hybrid AC/DC Microgrid and Its Coordination Control," *IEEE Trans. Smart Grid*, vol. 2, no. 2, pp. 278–286, June 2011.
- [11] N. Eghtedarpour and E. Farjah, "Power Control and Management in a Hybrid AC/DC Microgrid," *IEEE Trans. Smart Grid*, vol. 5, no. 3, pp. 1494–1505, May 2014.
- [12] F. Nejabatkhah and Y. W. Li, "Overview of Power Management Strategies of Hybrid AC/DC Microgrid," *IEEE Trans. Power Electron.*, vol. 30, no. 12, pp. 7072–7089, Dec 2015.
- [13] A. Hirsch, Y. Parag, and J. Guerrero, "Microgrids: A review of technologies, key drivers, and outstanding issues," *Renewable and Sustainable Energy Reviews*, vol. 90, pp. 402–411, 2018. [Online]. Available: <http://www.sciencedirect.com/science/article/pii/S136403211830128X>
- [14] A. A. Jabbar, A. Y. Elrayyah, M. Z. Wanik, A. P. Sanfilippo, and N. K. Singh, "Development of Hybrid AC/DC Laboratory-scale Smart Microgrid Testbed with Control Monitoring System Implementation in LabVIEW," in *2019 IEEE PES GTD Gd. Int. Conf. Expo. Asia, GTD Asia 2019*, may 2019, pp. 889–894.
- [15] Y. Khayat, Q. Shafiee, R. Heydari, M. Naderi, T. Dragičević, J. W. Simpson-Porco, F. Dörfler, M. Fathi, F. Blaabjerg, J. M. Guerrero, and H. Bevrani, "On the secondary control architectures of ac microgrids: An

overview," *IEEE Trans. Power Electron.*, vol. 35, no. 6, pp. 6482–6500, 2020.

- [16] J. W. Simpson-Porco, Q. Shafiee, F. Dörfler, J. C. Vásquez, J. M. Guerrero, and F. Bullo, "Secondary Frequency and Voltage Control of Islanded Microgrids via Distributed Averaging," *IEEE Trans. Ind. Electron.*, vol. 62, no. 11, pp. 7025–7038, Nov 2015.
- [17] L. Meng, X. Zhao, F. Tang, M. Savaghebi, T. Dragicevic, J. C. Vasquez, and J. M. Guerrero, "Distributed Voltage Unbalance Compensation in Islanded Microgrids by Using a Dynamic Consensus Algorithm," *IEEE Trans. Power Electron.*, vol. 31, no. 1, pp. 827–838, Jan 2016.
- [18] V. Nasirian, A. Davoudi, F. L. Lewis, and J. M. Guerrero, "Distributed Adaptive Droop Control for DC Distribution Systems," *IEEE Trans. Energy Convers.*, vol. 29, no. 4, pp. 944–956, Dec 2014.
- [19] S. K. Sahoo, A. K. Sinha, and N. K. Kishore, "Control Techniques in AC, DC, and Hybrid AC—DC Microgrid: A Review," *IEEE Trans. Emerg. Sel. Topics Power Electron.*, vol. 6, no. 2, pp. 738–759, June 2018.
- [20] E. A. A. Coelho, D. Wu, J. M. Guerrero, J. C. Vasquez, T. Dragičević, C. Stefanović, and P. Popovski, "Small-signal analysis of the microgrid secondary control considering a communication time delay," *IEEE Trans. Ind. Electron.*, vol. 63, no. 10, pp. 6257–6269, Oct 2016.
- [21] R. Zhang and B. Hredzak, "Distributed finite-time multiagent control for dc microgrids with time delays," *IEEE Trans. Smart Grid*, vol. 10, no. 3, pp. 2692–2701, May 2019.
- [22] P. C. Loh, D. Li, Y. K. Chai, and F. Blaabjerg, "Autonomous Control of Interlinking Converter With Energy Storage in Hybrid AC-DC Microgrid," *IEEE Trans. Ind. Appl.*, vol. 49, no. 3, pp. 1374–1382, May 2013.
- [23] P. Wang, C. Jin, D. Zhu, Y. Tang, P. C. Loh, and F. H. Choo, "Distributed Control for Autonomous Operation of a Three-Port AC/DC/DS Hybrid Microgrid," *IEEE Trans. Ind. Electron.*, vol. 62, no. 2, pp. 1279–1290, Feb 2015.
- [24] S. Peyghami, H. Mokhtari, and F. Blaabjerg, "Autonomous operation of a hybrid ac/dc microgrid with multiple interlinking converters," *IEEE Trans. Smart Grid*, vol. 9, no. 6, pp. 6480–6488, Nov 2018.
- [25] H. Yoo, T. Nguyen, and H. Kim, "Consensus-based distributed coordination control of hybrid ac/dc microgrids," *IEEE Trans. Sustain. Energy*, pp. 1–1, 2019.
- [26] S. Anand, B. G. Fernandes, and J. Guerrero, "Distributed Control to Ensure Proportional Load Sharing and Improve Voltage Regulation in Low-Voltage DC Microgrids," *IEEE Trans. Power Electron.*, vol. 28, no. 4, pp. 1900–1913, April 2013.
- [27] C. Jin, P. Wang, J. Xiao, Y. Tang, and F. H. Choo, "Implementation of Hierarchical Control in DC Microgrids," *IEEE Trans. Ind. Electron.*, vol. 61, no. 8, pp. 4032–4042, Aug 2014.
- [28] W. Yao, M. Chen, J. Matas, J. M. Guerrero, and Z. M. Qian, "Design and Analysis of the Droop Control Method for Parallel Inverters Considering the Impact of the Complex Impedance on the Power Sharing," *IEEE Trans. Ind. Electron.*, vol. 58, no. 2, pp. 576–588, Feb 2011.
- [29] J. S. Gómez, D. Sáez, J. W. Simpson-Porco, and R. Cárdenas, "Distributed predictive control for frequency and voltage regulation in microgrids," *IEEE Trans. Smart Grid*, vol. 11, no. 2, pp. 1319–1329, March 2020.
- [30] G. C. Verghese, I. J. Perez-Arriaga, and F. C. Schewpe, "Selective modal analysis with applications to electric power systems, part ii: The dynamic stability problem," *IEEE Trans. on Power Apparatus and Systems*, vol. PAS-101, no. 9, pp. 3126–3134, 1982.



**Enrique Espina** (S'17) was born in Santiago, Chile. In 2013, he received the B.Sc. degree in electrical engineering from the University of Santiago of Chile. In 2017, he received the M.Sc. degree in electrical engineering from the University of Chile.

Currently, Mr Espina is a Ph.D. candidate in electrical engineering under a double degree Cotutelle agreement between the University of Chile (Santiago, Chile) and the University of Waterloo (Waterloo, Ontario, Canada). He is currently a half-time Lecturer with the Department of Electrical

Engineering, University of Santiago of Chile, Santiago, Chile.

His main research interests include the control of hybrid ac/dc microgrids, energy storage systems, electrical vehicle technologies, renewable energies and power electronic converters.



**Roberto Cárdenas** (S'95-M'97-SM'07) was born in Punta Arenas, Chile. He received his B.S. degree from the University of Magallanes, Chile, in 1988 and his Msc. and Ph.D degrees from the University of Nottingham in 1992 and 1996 respectively. From 1989-1991 and 1996-2008 he was a lecturer in the University of Magallanes Chile. From 1991 to 1996 he was with the Power Electronics Machines and Control Group (PEMC group), University of Nottingham, United Kingdom. From 2009-2011 he was with the Electrical Engineering Department, University of Santiago. He is currently a full professor of power electronics and drives in the Electrical Engineering Department, University of Chile, Chile. His main interests are in control of electrical machines, variable speed drives and renewable energy systems. Prof. Cardenas is an Associate Editor for the IEEE TRANSACTIONS ON INDUSTRIAL ELECTRONICS.



**John W. Simpson-Porco** (S'10-M'15-) received the B.Sc. degree in engineering physics from Queen's University, Kingston, ON, Canada in 2010, and the Ph.D. degree in mechanical engineering from the University of California at Santa Barbara, Santa Barbara, CA, USA in 2015.

He is currently an Assistant Professor of Electrical and Computer Engineering at the University of Toronto, Toronto, ON, Canada. He was previously an Assistant Professor at the University of Waterloo, Waterloo, ON, Canada and a visiting scientist with the Automatic Control Laboratory at ETH Zürich, Zürich, Switzerland. His research focuses on feedback control theory and applications of control in modernized power grids.

Prof. Simpson-Porco is a recipient of the Automatica Paper Prize, the Center for Control, Dynamical Systems and Computation Best Thesis Award, and the IEEE PES Technical Committee Working Group Recognition Award for Outstanding Technical Report. He is currently an Associate Editor for the IEEE Transactions on Smart Grid.



**Doris Sáez** (S'93-M'96-SM'05) was born in Panguipulli, Chile. She received the M.Sc. and Ph.D. degrees in electrical engineering from the Pontificia Universidad Católica de Chile, Santiago, Chile, in 1995 and 2000, respectively. She is currently Full Professor with the Department of Electrical Engineering and the Head of the Indigenous People Program, Faculty of Mathematical and Physical Sciences, University of Chile, Santiago. She has coauthored the books *Hybrid Predictive Control for Dynamic Transport Problems* (Springer Verlag, 2013)

and *Optimization of Industrial Processes at Supervisory Level: Application to Control of Thermal Power Plants* (Springer-Verlag, 2002). Her research interests include predictive control, fuzzy control design, fuzzy identification, and control of microgrids. She serves as an Associate Editor for the IEEE Transactions on Smart Grid.



**Mehrdad Kazerani** (SM'02) received his B.Sc., Master's and PhD degrees in Electrical Engineering from Shiraz University, Iran (1980), Concordia University, Canada (1990), and McGill University, Canada (1995), respectively. From 1982 to 1987, he was with the Energy Ministry of Iran. He is presently a Professor with the Department of Electrical and Computer Engineering, University of Waterloo, Waterloo, Ontario, Canada. He is a registered professional engineer in the province of Ontario. His research interests include current-sourced converter

applications, matrix converters, distributed generation, energy storage, battery charging systems, transportation electrification and microgrids.